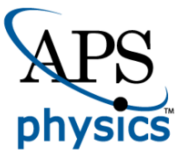

Enhanced superconductivity through virtual tunneling in Bernal bilayer graphene coupled to math xmlns="http://www.w3.org/1998/Math/MathML">msub>mi >WSe/mi>mn>2/mn>/msub>/math>

Yang-Zhi Chou, Fengcheng Wu, and Sankar Das Sarma

Phys. Rev. B **106**, L180502 — Published 3 November 2022

DOI: 10.1103/PhysRevB.106.L180502

Enhanced superconductivity through virtual tunneling in Bernal bilayer graphene coupled to WSe_2

Yang-Zhi Chou,[1,*] Fengcheng Wu,[2,3] and Sankar Das Sarma[1]

[1] *Condensed Matter Theory Center and Joint Quantum Institute, Department of Physics, University of Maryland, College Park, Maryland 20742, USA*
[2] *School of Physics and Technology, Wuhan University, Wuhan 430072, China*
[3] *Wuhan Institute of Quantum Technology, Wuhan 430206, China*

(Dated: October 25, 2022)

Motivated by a recent experiment [arXiv:2205.05087], we investigate a possible mechanism that enhances superconductivity in hole-doped Bernal bilayer graphene due to a proximate WSe_2 monolayer. We show that the virtual tunneling between WSe_2 and Bernal bilayer graphene, which is known to induce Ising spin-orbit coupling, can generate an additional attraction between two holes, providing a potential explanation for enhancing superconductivity in Bernal bilayer graphene. Using the microscopic interlayer tunneling, we derive the Ising spin-orbit coupling and the effective attraction as functions of the twist angle between Bernal bilayer graphene and WSe_2 monolayer. Our theory provides an intuitive and physical explanation for the intertwined relation between Ising spin-orbit coupling and superconductivity enhancement, which should motivate future studies.

Introduction.— Recent experiments on Bernal bilayer graphene (BBG) [1] and rhombohedral trilayer graphene (RTG) [2] reveal multiple symmetry broken phases and provide new understanding for superconductivity in general graphene systems (i.e., moiré [3–13] or moiréless systems [1, 2, 14]). In these non-moiré crystalline graphene multilayers, superconducting states with $T_c \leq 0.1$K are found in narrow regions close to interaction-driven "isospin" polarized phases [1, 2, 15]. Theoretically, the acoustic-phonon-mediated pairing can provide a consistent resolution for superconductivity in BBG and RTG [16–18], while interaction-driven mechanisms are also proposed [19–28].

A new experiment on superconductivity in BBG demonstrates that superconductivity can be significantly enhanced with a proximate WSe_2 [14]. The system consists of a WSe_2 monolayer on top of a BBG, and a displacement field (D) is used to control the layer-polarization of the low-energy bands. For a sufficiently large $D > 0$, the carriers of hole-doped BBG reside entirely on the top layer, and superconductivity is observed around 0.3K without a magnetic field. The superconducting state shows a nontrivial response to an in-plane magnetic field – Pauli-limit violation at lower doping and Pauli-limited behavior at higher doping. For $D < 0$, no superconductivity is observed for $T \geq 30$mK, but the normal states are essentially consistent with the previous experiment without a WSe_2 layer [1]. The striking different results for $D > 0$ and $D < 0$ suggest the significance of the proximate WSe_2 layer. It is important to emphasize that WSe_2 enhances superconductivity quite substantially – the superconducting temperature is enhanced by an order of magnitude (from 30mK to 300mK), the region of superconducting phase also becomes wider, and an in-plane magnetic field is no longer required to induce superconductivity.

The key task is to identify the physical origin of superconductivity enhancement. Since a small observable T_c has been found in BBG [1], any additional pairing glue or reduction of Coulomb repulsion can result in a noticeable enhancement in superconductivity. However, such a cooperative enhancing mechanism must be absent without a nearby WSe_2 layer, manifesting an asymmetric effect in $D > 0$ and $D < 0$. The main goal of the current work is to provide a potential explanation for the WSe_2-enhanced superconductivity in BBG [14].

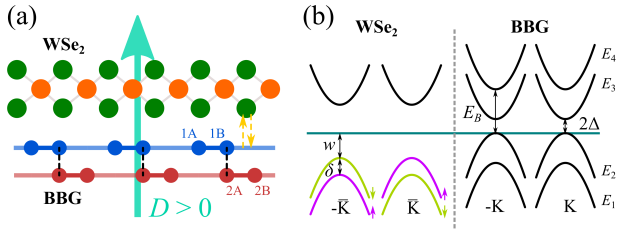

FIG. 1. Setup of BBG-WSe_2 and band structure. (a) Side view of the BBG-WSe_2 system. The WSe_2 monolayer is on top of the BBG. A displacement field along z-direction is exerted. (b) The schematic band structures of WSe_2 and BBG. The green line indicates the Fermi energy, which is on the band edge of the first BBG valence band (E_2). We ignore the spin splitting of the WSe_2 conduction bands in this illustration. We use E_1, E_2, E_3, and E_4 to label the BBG bands in ascending order in energy.

In this Letter, we propose a *novel* mechanism that enhances pairings in a BBG-WSe_2 system based on the interlayer tunneling between WSe_2 and BBG. Such a tunneling process is believed to induce Ising spin-orbit coupling (ISOC) in BBG [14, 29–32], implying significant interlayer tunneling. We develop a minimal theory that produces an effective attraction between two holes in the slightly hole-doped BBG via a virtual interlayer tunneling process in combination with interaction between hole carriers and the virtual electron. Furthermore, we derive

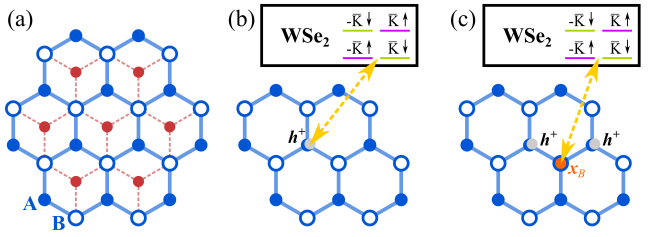

FIG. 2. Lattice model and virtual tunneling processes. (a) The effective honeycomb lattice model for BBG. A sites (blue dots) and B sites (blue opened circles) correspond to the positions of 1A and 1B sites in Fig. 1(a), respectively; the red dots indicate the 2B sites in the bottom graphene layer; 2A sites are right below the 1B sites. (b) ISOC due to virtual tunneling. (c) Attraction due to virtual tunneling.

the ISOC and effective attraction as functions of the relative angle between WSe_2 and BBG, incorporating microscopic tunneling at extended Brillouin zones [33, 34]. Our results suggest that the enhanced superconductivity can be explained by the virtual tunneling from WSe_2 layer in cooperation with electron-phonon interaction, paving the way for higher-T_c superconducting states in graphene systems.

Model.— We are interested in a BBG-WSe_2 system as depicted in Fig. 1. In the presence of a sufficiently large displacement field along z-direction ($D > 0$), the low-energy valence band of BBG is polarized at the 1A site [illustrated in Fig. 1(a)] on the top graphene layer. It was shown theoretically [31, 32] and experimentally [14, 29] that ISOC is induced primarily on the layer proximate to WSe_2, suggesting that tunneling between WSe_2 and the top graphene layer is essential. Thus, a minimal model must include certain properties of WSe_2 and BBG bands as well as the interlayer tunneling between WSe_2 and the top layer of BBG.

To simplify the problem, we consider an *effective* honeycomb model as follows (see Fig. 2 and [35]):

$$\hat{H}_{\rm tG} = E_A \sum_{\mathbf{r}_A} n(\mathbf{r}_A) + E_B \sum_{\mathbf{r}_B} n(\mathbf{r}_B), \qquad (1)$$

where E_A (E_B) corresponds to the onsite energy of the effective A (B) sites, $n(\mathbf{r}_\sigma) = \sum_{\tau,s} c^\dagger_{\tau\sigma s}(\mathbf{r}_\sigma) c_{\tau\sigma s}(\mathbf{r}_\sigma)$ is the number operator at site $\mathbf{r}_\sigma$, $c_{\tau\sigma s}$ is the fermionic annihilation operator with valley τK, sublattice $\sigma = A, B$, and spin s. The lack of hopping is because we consider momentum right at K or $-K$, where the system can be viewed as a collection of decoupled atomic sites. Equation (1) is a simplified description of BBG degrees of freedom relevant to the virtual tunneling processes considered in this work, and we retain only the E_2 band (A sites) and the E_4 band (B sites), where the E_2 and E_4 bands are labeled in Fig. 1(b). Due to the interlayer dimerization between 1B and 2A sites, the microscopic 1B sites of BBG are associated with both the E_1 and E_4 bands. For our proposal, the E_4 band is important, while the E_1 band is ignored. Thus, we consider $E_A = 0$ and set the value of E_B to the energy difference between the E_4 and the E_2 band edges [36], as illustrated in Fig. 1(b). In such a model, the charge neutral configuration [i.e., $\mathcal{E}_F$ is inside the 2Δ gap of Fig. 1(b)] corresponds to a state with completely filled A sites and empty B sites. In our case with $\mathcal{E}_F$ at the E_2 band edge, the system is slightly hole-doped, and we can consider ground states with dilute holes on the A sites of the effective honeycomb lattice model [given by Eq. (1)]. Again, the effective description here is valid when $\mathcal{E}_F$ is at the E_2 band edge.

In addition to the onsite potential, we consider electron-electron interactions given by

$$\hat{H}_I = \frac{U_0}{2} \sum_{\mathbf{r}} \delta n(\mathbf{r}) \left[\delta n(\mathbf{r}) - 1\right] + U_1 \sum_{\langle \mathbf{r}_A, \mathbf{r}_B \rangle} \delta n(\mathbf{r}_A) \delta n(\mathbf{r}_B), \quad (2)$$

where $\delta n(\mathbf{r}) = n(\mathbf{r}) - \langle 0|n(\mathbf{r})|0\rangle$, $|0\rangle$ is the state with a charge neutral configuration (i.e., filled A sites and empty B sites), $U_0 > 0$ ($U_1 > 0$) is the onsite (nearest-neighbor) Coulomb interaction, and $\langle \mathbf{r}_A, \mathbf{r}_B \rangle$ denotes the nearest-neighbor pair. We consider a sufficiently large U_0 such that at most one hole (electrons) can be created on sublattice A (B). U_1 term describes the interaction between nearest-neighbor sites, and $U_1 < E_B$ is assumed (as spontaneous formation of dipoles is forbidden). We will focus on the electron-hole attraction betweenan electron on B site and a hole on the nearest-neighbor A site in the virtual process.

The WSe_2 layer can be described by a semiconductor bandstructure with spin split valence bands [37] as illustrated in Fig. 1(b). Specifically, the energy splittings can be described by an ISOC, $\lambda \tau_z s_z$, with τ_z (s_z) being the z-component Pauli matrix for valley (spin). The interlayer tunneling between WSe_2 and BBG can facilitate spin-orbit splitting in BBG valence bands. To provide an intuitive understanding, we treat WSe_2 valence bands as a few representative energy levels described by a simplified Hamiltonian,

$$\hat{H}_d = -W\left(d^\dagger_{+,\uparrow} d_{+,\uparrow} + d^\dagger_{-,\downarrow} d_{-,\downarrow}\right) - (W+\delta)\left(d^\dagger_{-,\uparrow} d_{-,\uparrow} + d^\dagger_{+,\downarrow} d_{+,\downarrow}\right), \quad (3)$$

where $d_{\tau,s}$ denotes the fermionic annihilation operator with valley $\tau\bar{K}$ and spin s in the WSe_2 valence bands. W and δ are the parameters for the WSe_2 valence bands.

Finally, we consider a tunneling Hamiltonian between WSe_2 and BBG given by

$$\hat{H}_V = \sum_{\tau,s,\mathbf{r}_A} \left\{ c^\dagger_{\tau A s}(\mathbf{r}_A) \left[V^A_{\tau s} d_{\tau,s} + \bar{V}^A_{\tau s} d_{-\tau,s}\right] + \text{H.c.} \right\} + \sum_{\tau,s,\mathbf{r}_B} \left\{ c^\dagger_{\tau B s}(\mathbf{r}_B) \left[V^B_{\tau s} d_{\tau,s} + \bar{V}^B_{\tau s} d_{-\tau,s}\right] + \text{H.c.} \right\}, \quad (4)$$

where $V^\sigma_{\tau s}$ is the tunneling strength for the intravalley process (i.e., $\tau\bar{K}$ to τK), $\bar{V}^\sigma_{\tau s}$ is the tunneling strength

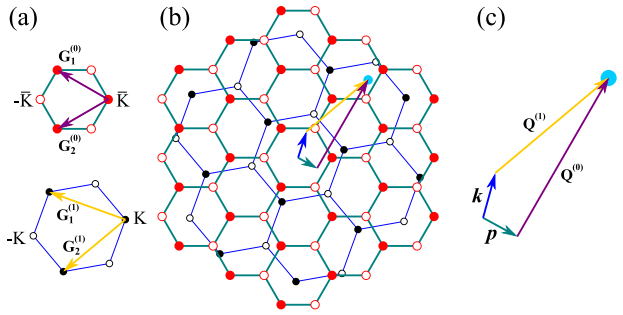

FIG. 3. Brillouin zone and geometry of interlayer tunneling. (a) First Brillouin zone of WSe_2 (green) and BBG (blue). BBG is rotated by a twist angle θ. We use $\theta = 10^\circ$ here. $\mathbf{G}_a^{(0)}$'s and $\mathbf{G}_a^{(1)}$'s are the primitive lattice vectors of reciprocal lattice of WSe_2 and BBG, respectively. (b) Extended Brillouin zones. (c) Momenta $\mathbf{p}$ and $\mathbf{k}$ have the same crystal momentum as $\mathbf{p}+\mathbf{Q}^{(0)} = \mathbf{k}+\mathbf{Q}^{(1)}$, where $\mathbf{Q}^{(0)}$ and $\mathbf{Q}^{(1)}$ are the reciprocal lattice vectors of WSe_2 and BBG, respectively.

for the intervalley process (i.e., $-\tau\bar{K}$ to τK) [38]. Since the entire system preserves the (spinful) time-reversal symmetry, the tunneling terms obey $|V^\sigma_{\bar{\tau}\bar{s}}| = |V^\sigma_{\tau s}|$ and $\left|\bar{V}^\sigma_{\bar{\tau}\bar{s}}\right| = \left|\bar{V}^\sigma_{\tau s}\right|$, where $\bar{\tau}$ ($\bar{s}$) means the time-reversal partner of τ (s).

The model designed here is physically motivated for understanding ISOC and effective attraction via interlayer tunneling. However, such a simplified model cannot capture the full microscopic detail. We will later use a detailed approach incorporating WSe_2 band structures and the microscopic interlayer tunneling matrix elements.

Ising spin-orbit coupling and effective attraction.— The minimal model $\hat{H} = \hat{H}_{\rm tG} + \hat{H}_I + \hat{H}_d + \hat{H}_V$ [given by Eqs. (1), (2), (3), and (4)] can straightforwardly produce ISOC in the first valence band of BBG. The main idea is that the second-order perturbation in $\hat{H}_V$ as sketched in Fig. 2(b) (see also [35]) generates spin-valley-splitting energy levels on A sites, realizing an ISOC with strength

$$\lambda_I = \frac{\left|V^A_{+\uparrow}\right|^2 - \left|\bar{V}^A_{+\uparrow}\right|^2}{W} - \frac{\left|V^A_{+\downarrow}\right|^2 - \left|\bar{V}^A_{+\downarrow}\right|^2}{W+\delta}. \tag{5}$$

The main goal of this work is to investigate if the interlayer tunneling between WSe_2 and BBG can generate an effective attractive interaction. Specifically, we consider two holes that contain a common nearest-neighbor B site at $\mathbf{x}_B$ as illustrated in Fig. 2(c). At the second-order perturbation of $\hat{H}_V$, the interplay between virtual tunneling and the interaction $\hat{H}_I$ [Eq. (2)] generates an effective attraction between the holes, described by [35]

$$\hat{H}_{\rm att} = -\mathcal{U}_{\rm eff} \sum_{\langle\langle \mathbf{r}_A, \mathbf{r}'_A\rangle\rangle} \delta n(\mathbf{r}_A)\delta n(\mathbf{r}'_A), \tag{6}$$

where the sum runs over the nearby pairs on A sites and

$$\begin{aligned}\mathcal{U}_{\rm eff} = &\frac{\mathcal{V}^2_\uparrow}{W+E_B} + \frac{\mathcal{V}^2_\uparrow}{W+E_B-2U_1} - \frac{2\mathcal{V}^2_\uparrow}{W+E_B-U_1} \\ &+ \frac{\mathcal{V}^2_\downarrow}{W+\delta+E_B} + \frac{\mathcal{V}^2_\downarrow}{W+\delta+E_B-2U_1} - \frac{2\mathcal{V}^2_\downarrow}{W+\delta+E_B-U_1}\end{aligned} \tag{7}$$

with $\mathcal{V}^2_s = 2\left|V^B_{+s}\right|^2 + 2\left|\bar{V}^B_{+s}\right|^2$. $\mathcal{U}_{\rm eff}$ vanishes as U_1 is absent. While the electron on a B site has a large local energy E_B, the nearest-neighbor electron-hole attraction can lower the total energy in a virtual state. In Eq. (7), those terms with $-2U_1$, corresponding to virtual tunneling to $\mathbf{x}_B$, yield the dominant contributions as long as $U_1 > 0$. We assume that $W + E_B > 2U_1$ so that the any charge transfer between WSe_2 and BBG should be absent. Since $|V^A_{\tau s}|$ and $|V^B_{\tau s}|$ are of the same order of magnitude [35], we expect that the virtual tunneling generates a sizable effective attraction $\mathcal{U}_{\rm eff}$. Our theory therefore provides an intuitive understanding of the effective attraction due to a proximate WSe_2 layer.

The proposed mechanism here is conceptually related to the "polarizer" idea [39, 40] and the repulsion-induced attraction in models on honeycomb lattice [41–44]. We discuss a few differences between our work and Refs. [41–44] – (i) the virtual process is due to interlayer tunneling rather than intralayer hopping, and (ii) electron-hole attraction in the virtual process rather than electron-electron repulsion. The point (i) is crucial as our mechanism describes a possible enhanced attraction from WSe_2 rather than pairings due to intralayer processes. In addition, the point (ii) allows for a wider parameter range for a sizable effective attraction because the large onsite energy E_B can be compensated by nearest neighbor attraction.

Interlayer tunneling and twist angle.— The interlayer tunneling between WSe_2 and BBG crucially determines ISOC as well as the virtual-tunneling-induced effective attraction. The interlayer tunneling preserves crystal momentum as the matrix element primarily depends on the distance between the sites. Within the two-center approximation scheme, the tunneling between the layers can be described by [33]

$$\begin{aligned}T^{\alpha,\sigma;\beta,\sigma'}_{\mathbf{k},\mathbf{p}} = &\frac{1}{\sqrt{\mathcal{A}_0\mathcal{A}_1}} \left(a^{(1)}_{\mathbf{k},\alpha,\sigma}\right)^* \left(a^{(0)}_{\mathbf{p},\beta,\sigma'}\right) \times \\ &\sum_{\mathbf{Q}^{(1)},\mathbf{Q}^{(0)}} \tilde{t}_{\mathbf{k}+\mathbf{Q}^{(1)}} e^{i\phi^{\sigma;\sigma'}_{\mathbf{Q}^{(1)},\mathbf{Q}^{(0)}}} \delta_{\mathbf{k}+\mathbf{Q}^{(1)},\mathbf{p}+\mathbf{Q}^{(0)}},\end{aligned} \tag{8}$$

where $\mathcal{A}_0$ ($\mathcal{A}_1$) is the unit-cell area of WSe_2 (BBG), α and β are the band indexes, $\mathbf{k}$ of BBG and $\mathbf{p}$ of WSe_2 are the momentum relative to Γ point (Brillouin zone center), σ and σ' are the sublattice (orbital) indexes, $a^{(l)}_{\mathbf{k},\alpha,\sigma}$ is the sublattice (orbital) projection of a Bloch state $|\mathbf{k},\alpha\rangle$ at layer l, and $\mathbf{Q}^{(0)}$, $\mathbf{Q}^{(1)}$ are the reciprocal lattice vectors

in WSe_2 and BBG, respectively, and $\phi^{\sigma;\sigma'}_{\mathbf{Q}^{(1)},\mathbf{Q}^{(0)}}$ is a phase factor depending on sublattice. In the above expression, we use index 0 for the WSe_2 layer and index 1 for the top graphene layer of BBG. $\tilde{t}_{\mathbf{k}}$ is the 2D Fourier transform of the interlayer tunneling amplitude with a finite range, and we use a stretched exponential ansatz form [33],

$$|\tilde{t}_{\mathbf{k}}| = t_0 e^{-\chi(|\mathbf{k}|z_\perp)^\gamma}, \tag{9}$$

where t_0 is an overall constant, χ is an order 1 numerical constant, γ is the exponent of stretched exponential, and $z_\perp$ is the distance between WSe_2 monolayer and the top graphene layer of BBG [45]. Note that Eq. (9) is an empirical expression for a finite $\mathbf{k}$, and the potential complications for $\mathbf{k} \to 0$ are not relevant to our problem.

The interlayer tunneling described by Eq. (8) is a highly nontrivial single-particle process. Microscopically, WSe_2 and BBG have a relative angle that is tunable experimentally as well as different lattice constants ($d = 3.31$Å for WSe_2, $a = 2.46$Å for BBG), resulting in Brillouin zones illustrated in Fig. 3. Note that $T^{\alpha,\sigma;\beta,\sigma'}_{\mathbf{k},\mathbf{p}}$ is nonzero as long as $\mathbf{k} + \mathbf{Q}^{(1)} = \mathbf{p} + \mathbf{Q}^{(0)}$ for some reciprocal lattice vectors $\mathbf{Q}^{(0)}$ and $\mathbf{Q}^{(1)}$. Thus, a full calculation must incorporate a sufficiently large number of extended Brillouin zones. Using the virtual-tunneling ideas discussed previously, we can compute the λ_I and $\mathcal{U}_{\text{eff}}$ incorporating the microscopic interlayer tunneling matrix elements between the $\mathbf{k}\cdot\mathbf{p}$ WSe_2 bands [37] and our honeycomb model. We summarize main results, and the complete derivations are provided in [35].

In Fig. 4, we plot the twist-angle (θ) dependence of λ_I with a few representative values of χ and γ [46]. λ_I is generally positive for small positive θ and becomes negative slightly above $\theta = 15°$. Moreover, nonmonotonic behavior can manifest near $\theta = 5°$ and $\theta = 20°$ for smaller γ and χ. These results can be understood by the geometry of momentum at $\theta = 5°$ and $\theta \geq 20°$ [35]. At $\theta = 30°$, λ_I vanishes because the intervalley and intravalley tunnelings have exactly the same contributions. Similar nonmonotonic behavior near $\theta = 20°$ was also theoretically reported in graphene coupled to transition metal dichalcogenide [34, 47, 48]. In addition, the sign changing in λ_I (curves with $\gamma = 1$ in Fig. 4) was also obtained in Ref. [34]. In Fig. 5, we plot the θ dependence of $\mathcal{U}_{\text{eff}}$ with $U_1 = 0.3$eV and $U_1 = 0.43$eV (the largest possible value in our theory) and a few different values of χ and γ. $\mathcal{U}_{\text{eff}}$ is generally larger at smaller θ, but nonmonotonic features might develop for small γ and χ. While the qualitative results are insensitive to U_1, the quantitative values depend on U_1 [35]. An important implication here is that ISOC strength and the effective attraction are *not* directly related to each other. The full results depend a lot on the details of $T^{\alpha,\sigma;\beta,\sigma'}_{\mathbf{k},\mathbf{p}}$.

Discussion.— The virtual-tunneling-induced attraction might explain the enhanced superconductivity in BBG-WSe_2 [14] as it enters the theory nonperturbatively

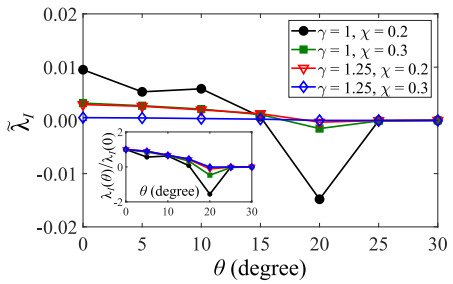

FIG. 4. Ising spin-orbit coupling versus twist angle (θ) with microscopic interlayer tunneling. We plot the dimensionless spin-orbit coupling $\tilde{\lambda}_I = \lambda_I \mathcal{A}_0 \mathcal{A}_1 \text{eV}/t_0^2$ as a function of θ with different values of γ and χ. $W = 0.62$eV and $\delta = 0.46$eV for all the plots.

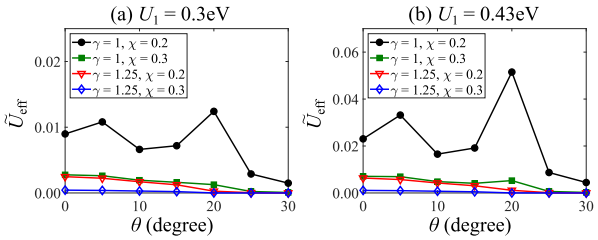

FIG. 5. Effective attraction versus twist angle (θ) with microscopic interlayer tunneling. We plot the dimensionless spin-orbit coupling $\tilde{U}_{\text{eff}} = \mathcal{U}_{\text{eff}} \mathcal{A}_0 \mathcal{A}_1 \text{eV}/t_0^2$ as a function of θ with different values of γ, χ, and U_1. (a) $U_1 = 0.3$eV. (b) $U_1 = 0.43$eV. $W = 0.62$eV and $\delta = 0.46$eV for all the plots.

in an exponential function determining T_c and the effect is primarily on $D > 0$. In the BBG experiment without WSe_2 [1], superconductivity with $T_c \sim 30$mK was reported at the doping density $n_e = -6 \times 10^{12}\text{cm}^{-2}$ with a Fermi-surface degeneracy factor of 2, implying that pairing interaction between holes overcomes Coulomb suppression. Since the enhanced superconductivity is found near the same doping density with a very similar Fermi-surface degeneracy factor, we anticipate that the same pairing mechanism manifests in BBG with or without the proximate WSe_2. According to Ref. [17], the acoustic-phonon-mediated attraction is slightly stronger than the Coulomb suppression, so any additional pairing glue due to presence of WSe_2, albeit small compared to the Coulomb repulsion, might considerably enhance superconductivity because T_c is exponentially related to the coupling constant. As such, our theory based on interplay between virtual tunneling and interaction is a possible explanation for the BBG-WSe_2 experiment [14]. We also derive the twist-angle dependence of the ISOC parameter and the effective attraction, providing guidance for future BBG-WSe_2 systems.

It is worth mentioning that our theory most likely underestimates $\mathcal{U}_{\text{eff}}$ because we consider only the nearest-neighbor Coulomb interaction and only valley momenta (i.e., K and $-K$ points) in the BBG bands. With a

long-range Coulomb interaction, long-range effective attraction can also arise from virtual tunneling processes, resulting in an overall stronger pairing. Moreover, incorporating all the allowed momenta in the BBG E_4 band also enhances $\mathcal{U}_{\text{eff}}$ because there are more states to be tunneled into.

Now we discuss the pairing symmetry and the normal state in BBG-WSe_2 system. We anticipate that intervalley intrasublattice pairings dominate [16, 49, 50] because of the layer-sublattice polarization in BBG. Based on the previous work on acoustic phonons [17] and the ideas discussed in this Letter, we assume that the dominant pairing is due to the acoustic phonons, and the virtual-tunneling-induced attraction is the subleading pairing glue. Note that the normal states for superconductivity in Refs. [1] and [14] are qualitatively different due to the differences in spin-orbit coupling and the in-plane magnetic field. While our theory does not determine the normal state properties, the major pairing glue, the acoustic-phonon-mediated pairing, has a $SU(2) \times SU(2)$ symmetry [16, 17, 49] (allowing for singlet, triplet, and singlet-triplet mixing). Thus, the superconductivity should be enhanced regardless of the details of the spin symmetry in normal state or in the subleading pairing [51]. Due to the induced spin-orbit coupling, we anticipate an admixture of singlet and triplet pairings [52, 53], which can produce a beyond-Pauli-limit response to the in-plane magnetic field, consistent with the lower-doping superconductivity in the BBG-WSe_2 experiment [14].

While our theory provides a potential consistent resolution to the BBG-WSe_2 experiment, there are a few issues that require further investigations. First, the effective attraction $\mathcal{U}_{\text{eff}}$ depends on the value of U_1, which we treat as a parameter. This makes a quantitative estimate of $\mathcal{U}_{\text{eff}}$ difficult in our theory. The other issue is related to the differences in the normal states between Refs. [1] and [14]. In our work, we simply assume that such differences are not crucial to the superconductivity enhancement. However, as pointed out in Ref. [14], a nontrivial normal state due to an interplay between interaction and spin orbit coupling might explain the enhancement of superconductivity. To fully understand the factor-of-10 enhancement of T_c in the BBG-WSe_2 experiment [14], one needs to incorporate both the additional pairing glue and the change in normal states.

Finally, we discuss implications for experiments. First, the twist-angle dependence of ISOC [Fig. 4] and effective attraction [Fig. 5] might provide insights on why enhanced superconductivity is not always achieved in BBG-WSe_2 experiments [14]. Based on our theory, applying a pressure to the system should considerably raise T_c since an applied pressure should enhance tunneling. Furthermore, one can use the ideas of this work to look for the optimal proximate layer for enhancing superconductivity. An important message of this work is that superconductivity can still be enhanced even if the induced spin-orbit coupling is very small, because of the exponential nature in T_c and the complex relation between effective attraction and spin-orbit coupling.

Acknowledgments.— We thank Étienne Lantagne-Hurtubise, Alex Thomson, and Cyprian Lewandowski for pointing out an issue in the earlier version of manuscript. We are also grateful to Seth Davis, Jiabin Yu, and Ming Xie for useful discussions. This work is supported by the Laboratory for Physical Sciences (Y.-Z.C. and S.D.S.), by JQI-NSF-PFC (Y.-Z.C.), and by ARO W911NF2010232 (Y.-Z.C.). F.W. is supported by National Key R&D Program of China 2021YFA1401300 and start-up funding of Wuhan University.

* yzchou@umd.edu

[1] H. Zhou, L. Holleis, Y. Saito, L. Cohen, W. Huynh, C. L. Patterson, F. Yang, T. Taniguchi, K. Watanabe, and A. F. Young, Science **375**, 774 (2022).
[2] H. Zhou, T. Xie, T. Taniguchi, K. Watanabe, and A. F. Young, Nature **598**, 434 (2021).
[3] Y. Cao, V. Fatemi, S. Fang, K. Watanabe, T. Taniguchi, E. Kaxiras, and P. Jarillo-Herrero, Nature **556**, 43 (2018), URL `http://dx.doi.org/10.1038/nature26160`.
[4] M. Yankowitz, S. Chen, H. Polshyn, Y. Zhang, K. Watanabe, T. Taniguchi, D. Graf, A. F. Young, and C. R. Dean, Science **363**, 1059 (2019).
[5] X. Lu, P. Stepanov, W. Yang, M. Xie, M. A. Aamir, I. Das, C. Urgell, K. Watanabe, T. Taniguchi, G. Zhang, et al., Nature **574**, 653 (2019).
[6] Z. Hao, A. Zimmerman, P. Ledwith, E. Khalaf, D. H. Najafabadi, K. Watanabe, T. Taniguchi, A. Vishwanath, and P. Kim, Science **371**, 1133 (2021).
[7] J. M. Park, Y. Cao, K. Watanabe, T. Taniguchi, and P. Jarillo-Herrero, Nature **590**, 249 (2021).
[8] Y. Cao, J. M. Park, K. Watanabe, T. Taniguchi, and P. Jarillo-Herrero, Nature **595**, 526 (2021).
[9] X. Liu, K. Watanabe, T. Taniguchi, and J. Li, arXiv preprint arXiv:2108.03338 (2021).
[10] Y. Zhang, R. Polski, C. Lewandowski, A. Thomson, Y. Peng, Y. Choi, H. Kim, K. Watanabe, T. Taniguchi, J. Alicea, et al., arXiv preprint arXiv:2112.09270 (2021).
[11] J. M. Park, Y. Cao, L. Xia, S. Sun, K. Watanabe, T. Taniguchi, and P. Jarillo-Herrero, arXiv preprint arXiv:2112.10760 (2021).
[12] G. W. Burg, E. Khalaf, Y. Wang, K. Watanabe, T. Taniguchi, and E. Tutuc, arXiv preprint arXiv:2201.01637 (2022).
[13] P. Siriviboon, J. Lin, X. Liu, H. Scammell, S. Liu, D. Rhodes, K. Watanabe, T. Taniguchi, J. Hone, M. Scheurer, et al., arXiv preprint arXiv:2112.07127 (2021).
[14] Y. Zhang, R. Polski, A. Thomson, É. Lantagne-Hurtubise, C. Lewandowski, H. Zhou, K. Watanabe, T. Taniguchi, J. Alicea, and S. Nadj-Perge, arXiv preprint arXiv:2205.05087 (2022).
[15] H. Zhou, T. Xie, A. Ghazaryan, T. Holder, J. R. Ehrets, E. M. Spanton, T. Taniguchi, K. Watanabe, E. Berg,

M. Serbyn, et al., Nature **598**, 429 (2021).
[16] Y.-Z. Chou, F. Wu, J. D. Sau, and S. Das Sarma, Phys. Rev. Lett. **127**, 187001 (2021), URL https://link.aps.org/doi/10.1103/PhysRevLett.127.187001.
[17] Y.-Z. Chou, F. Wu, J. D. Sau, and S. Das Sarma, Phys. Rev. B **105**, L100503 (2022), URL https://link.aps.org/doi/10.1103/PhysRevB.105.L100503.
[18] Y.-Z. Chou, F. Wu, J. D. Sau, and S. Das Sarma, arXiv preprint arXiv:2204.09811 (2022).
[19] S. Chatterjee, T. Wang, E. Berg, and M. P. Zaletel, arXiv preprint arXiv:2109.00002 (2021).
[20] A. Ghazaryan, T. Holder, M. Serbyn, and E. Berg, Phys. Rev. Lett. **127**, 247001 (2021), URL https://link.aps.org/doi/10.1103/PhysRevLett.127.247001.
[21] Z. Dong and L. Levitov, arXiv preprint arXiv:2109.01133 (2021).
[22] T. Cea, P. A. Pantaleón, V. o. T. Phong, and F. Guinea, Phys. Rev. B **105**, 075432 (2022), URL https://link.aps.org/doi/10.1103/PhysRevB.105.075432.
[23] A. L. Szabó and B. Roy, Phys. Rev. B **105**, L081407 (2022), URL https://link.aps.org/doi/10.1103/PhysRevB.105.L081407.
[24] Y.-Z. You and A. Vishwanath, Phys. Rev. B **105**, 134524 (2022), URL https://link.aps.org/doi/10.1103/PhysRevB.105.134524.
[25] W. Qin, C. Huang, T. Wolf, N. Wei, I. Blinov, and A. H. MacDonald, arXiv preprint arXiv:2203.09083 (2022).
[26] H. Dai, R. Ma, X. Zhang, and T. Ma, arXiv preprint arXiv:2204.06222 (2022).
[27] A. L. Szabó and B. Roy, Phys. Rev. B **105**, L201107 (2022), URL https://link.aps.org/doi/10.1103/PhysRevB.105.L201107.
[28] Z. Dong, A. V. Chubukov, and L. Levitov, arXiv preprint arXiv:2205.13353 (2022).
[29] J. Island, X. Cui, C. Lewandowski, J. Khoo, E. Spanton, H. Zhou, D. Rhodes, J. Hone, T. Taniguchi, K. Watanabe, et al., Nature **571**, 85 (2019).
[30] M. Gmitra, D. Kochan, P. Högl, and J. Fabian, Phys. Rev. B **93**, 155104 (2016), URL https://link.aps.org/doi/10.1103/PhysRevB.93.155104.
[31] M. Gmitra and J. Fabian, Phys. Rev. Lett. **119**, 146401 (2017), URL https://link.aps.org/doi/10.1103/PhysRevLett.119.146401.
[32] J. Y. Khoo, A. F. Morpurgo, and L. Levitov, Nano letters **17**, 7003 (2017).
[33] R. Bistritzer and A. H. MacDonald, Phys. Rev. B **81**, 245412 (2010), URL https://link.aps.org/doi/10.1103/PhysRevB.81.245412.
[34] A. David, P. Rakyta, A. Kormányos, and G. Burkard, Phys. Rev. B **100**, 085412 (2019), URL https://link.aps.org/doi/10.1103/PhysRevB.100.085412.
[35] See supplemental material.
[36] In this work, we use $E_B = \sqrt{t_1^2 + \Delta^2} + \Delta + \Delta'$, where t_1 denotes the interlayer dimerization energy between the 1B and 2A sites of BBG, Δ is the potential energy induced by the displacement field, Δ' is the local potential shift at 1B and 2A sites of BBG. (See Ref. [54] and Supplementary Material for the values used in this work [35].).
[37] D. Xiao, G.-B. Liu, W. Feng, X. Xu, and W. Yao, Phys. Rev. Lett. **108**, 196802 (2012), URL https://link.aps.org/doi/10.1103/PhysRevLett.108.196802.
[38] In principle, the tunneling strength should vary in space because the WSe_2 layer and top graphene layer of BBG can form a moiré pattern. However, the BBG-WSe_2 system has a mean free path of order of sample size [14], suggesting that the spatial dependence is not essential. Thus, we ignore the spatial dependence in $V_{\tau s}^{\sigma}$ and $\bar{V}_{\tau s}^{\sigma}$.
[39] W. A. Little, Phys. Rev. **134**, A1416 (1964), URL https://link.aps.org/doi/10.1103/PhysRev.134.A1416.
[40] A. Hamo, A. Benyamini, I. Shapir, I. Khivrich, J. Waissman, K. Kaasbjerg, Y. Oreg, F. von Oppen, and S. Ilani, Nature **535**, 395 (2016).
[41] K. Slagle and L. Fu, Phys. Rev. B **102**, 235423 (2020), URL https://link.aps.org/doi/10.1103/PhysRevB.102.235423.
[42] V. Crépel and L. Fu, Science Advances **7**, eabh2233 (2021).
[43] V. Crépel and L. Fu, Proceedings of the National Academy of Sciences **119**, e2117735119 (2022).
[44] V. Crépel, T. Cea, L. Fu, and F. Guinea, Phys. Rev. B **105**, 094506 (2022), URL https://link.aps.org/doi/10.1103/PhysRevB.105.094506.
[45] For simplicity, we assume $z_\perp = 3.34$Å, the same as the distance between two graphene layers. The interlayer distance dependence can be absorbed into the parameter χ.
[46] In Ref. [33], $\gamma = 1.25$ and $\chi = 0.13$ were used for twisted bilayer graphene. We assume that γ and χ here are not significantly different from those values.
[47] Y. Li and M. Koshino, Phys. Rev. B **99**, 075438 (2019), URL https://link.aps.org/doi/10.1103/PhysRevB.99.075438.
[48] T. Naimer, K. Zollner, M. Gmitra, and J. Fabian, Phys. Rev. B **104**, 195156 (2021), URL https://link.aps.org/doi/10.1103/PhysRevB.104.195156.
[49] F. Wu, E. Hwang, and S. Das Sarma, Phys. Rev. B **99**, 165112 (2019), URL https://link.aps.org/doi/10.1103/PhysRevB.99.165112.
[50] Y.-Z. Chou, F. Wu, J. D. Sau, and S. Das Sarma, Phys. Rev. Lett. **127**, 217001 (2021), URL https://link.aps.org/doi/10.1103/PhysRevLett.127.217001.
[51] The $\mathcal{U}_{\text{eff}}$ interaction [Eq. (7)] preserves $SU(2) \times SU(2)$ symmetry, but this is an artifact of our minimal model. Usually, the short-range interaction preserves only the global $SU(2)$ symmetry, and the higher-order contributions involving both V_A and V_B tunnelings break the spin symmetry entirely.
[52] J. Lu, O. Zheliuk, I. Leermakers, N. F. Yuan, U. Zeitler, K. T. Law, and J. Ye, Science **350**, 1353 (2015).
[53] X. Xi, Z. Wang, W. Zhao, J.-H. Park, K. T. Law, H. Berger, L. Forró, J. Shan, and K. F. Mak, Nature Physics **12**, 139 (2016).
[54] J. Jung and A. H. MacDonald, Phys. Rev. B **89**, 035405 (2014), URL https://link.aps.org/doi/10.1103/PhysRevB.89.035405.